# Macromolecules

Article

Tailored Self-Assembled Ferroelectric Polymer Nanostructures with Tunable Response

Ivan Terzic,[†] Niels L. Meereboer,[†] Mónica Acuautla,[‡] Giuseppe Portale,[†] and Katja Loos[*,†]

[†]Macromolecular Chemistry and New Polymeric Materials and [‡]Nanostructures of Functional Oxides, Zernike Institute for Advanced Materials, University of Groningen, Nijenborgh 4, 9747AG Groningen, The Netherlands

S Supporting Information

ABSTRACT: A facile ferroelectric nanostructures preparation method is developed based on the self-assembly of poly(2-vinylpyridine)-b-poly(vinylidene fluoride-co-trifluoroethylene)-b-poly(2-vinylpyridine) triblock copolymers (P2VP-b-P(VDF-TrFE)-b-P2VP), and the effect of morphological characteristics of the block copolymers on the ferroelectric response has been investigated for the first time. By simple adjustment of the ratio between the blocks, lamellar, cylindrical, and spherical morphologies are obtained in the melt and preserved upon crystallization of P(VDF-TrFE). However, at high P(VDF-TrFE) content, crystallization becomes dominant and drives the self-assembly of block copolymers. The crystallization study of the block copolymers reveals the preservation of the high degree of crystallinity inside the confined nanodomains as well as the reduction of the crystalline size and the Curie transition temperature with the confinement level. Only a small difference in the coercive field and the shape of the hysteresis loop is observed for block copolymers with a lamellar morphology produced either by crystallization-driven self-assembly or by confinement inside preformed lamellar domains. In contrast, delayed spontaneous polarization or the absence of dipole switching is demonstrated for the confinement of ferroelectric crystals inside both isolated cylindrical and spherical domains, exemplifying the influence of dimensionality on the critical size for ferroelectric order.
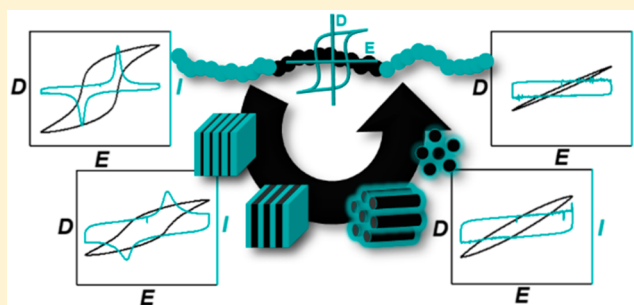
INTRODUCTION

The ever-growing expansion of flexible electronics has led to a great interest in ferroelectric polymers, especially poly-(vinylidene fluoride) (PVDF) and its copolymer with trifluoroethylene (PVDF-TrFE).[1−3] Even though demonstrating lower spontaneous polarization, dielectric constants, and piezoelectric coefficients compared to the conventional ferroelectric ceramics (e.g., $BaTiO_3$ and lead zirconate titanate (PZT)), their high flexibility, excellent low-temperature processability, light weight, and biocompatibility make them perfect candidates for a great variety of applications, including data storage, energy harvesting, sensing and actuation, field-effect transistors, and solar cells.[4−9] Recently, much research attention has been dedicated to the fabrication of nanostructured ferroelectric polymers with the goal of improving their properties.[4,7,10] It has been demonstrated that confinement of a ferroelectric polymer inside nanodomains favors the formation of the ferroelectric phase and leads to a preferential orientation of the polymer chains, providing easier dipole switching.[11] So far, confinement is mostly accomplished using nanoporous alumina or orthosilicate templates and nanoimprinting.[12−14] However, long fabrication times and the inability of mass production prevent wider use of the template method for the preparation of ferroelectric nanostructures, while the still expensive and complicated production of imprint molds presents the main drawback for the implementation of

nanoimprint lithography. In contrast, self-assembly, whereby organized nanostructures are formed as a consequence of specific interactions inside the material with the aim to reduce the free energy of the system, has arisen as one of the simplest procedures for polymer nanostructure preparation.[15−17]

Block copolymers, because of the covalent link between the blocks as well as their immiscibility, can microphase separate on a molecular level (10−100 nm), producing different well-ordered morphologies.[18] For AB or ABA block copolymers with narrow molecular weight distribution, spherical, cylindrical, lamellar, and even bicontinuous gyroid structures have been obtained, while incorporating a third block or increasing dispersity leads to even richer phase behavior.[19,20] Contrary to the previously mentioned methods for nanostructure preparation, the nanostructure shape and size can be easily tuned by changing the ratio between blocks and their molecular weight.[21] Furthermore, the already formed morphologies can be well aligned over a large area using various methods.[22−24]

Introduction of a crystalline block can make the phase separation process more complex due to the competition between crystallization and microphase separation.[25−27] After melting the crystalline component in the crystalline−

amorphous block copolymer, phase separation proceeds in the same way as for amorphous–amorphous block copolymers. However, after the block copolymer system is cooled below the crystallization temperature of the semicrystalline block, several different scenarios can occur, depending on the molecular structure of the blocks.[28] In the case of weakly segregated block copolymers, or block copolymers with low glass transition temperature (T_g) of the amorphous block, the preformed morphology is replaced with crystalline lamellae consisting of alternating crystalline and amorphous layers (breakout crystallization).[29,30] Conversely, strong phase separation, together with a high T_g, guides the crystal formation inside nanodomains, preserving the morphology formed in the melt (confined crystallization).[31]

Even though the constant increase of PVDF and P(VDF-TrFE) applications is observed in many fields, the study of their block copolymer self-assembly is limited, mainly due to the lack of synthetic procedures but also to molecular weight limitations of controlled radical polymerization techniques employed for the preparation of PVDF-based block copolymers.[27,29,30,32,33] No phase separation in the melt and a lamellar structure, which is a result of crystallization-driven self-assembly, can be detected in most cases.[27,29,34] Recently, our group has reported the use of the copper(I)-catalyzed azide–alkyne cycloaddition reaction for the synthesis of the poly(2-vinylpyridine)-*b*-PVDF-*b*-poly(2-vinylpyridine) and poly(2-vinylpyridine)-*b*-P(VDF-TrFE)-*b*-poly(2-vinylpyridine) block copolymers that demonstrated good phase separation in the molten state and strong influence of the block copolymer morphology on the formed crystalline phase of PVDF.[35,36] Moreover, it has been proven that the incorporation of the polar poly(2-vinylpyridine) (P2VP) does not impede the ferroelectricity inside the P2VP-*b*-P(VDF-TrFE)-*b*-P2VP block copolymer with 30 wt % P2VP. Nevertheless, no detailed study of the microphase separation of this block copolymer system is reported, and the understanding of the structure–ferroelectric response relationship is not yet accomplished.

In the current work, we focus on investigating the self-assembly behavior of P2VP-*b*-P(VDF-TrFE)-*b*-P2VP block copolymers. With increasing the P(VDF-TrFE) content in the block copolymers, spherical, hexagonally packed cylindrical and lamellar structures are obtained in the melt and are retained after crystallization. However, no ordered morphology is detected for block copolymers with P(VDF-TrFE) as the major component. On the contrary, crystallization-driven self-assembly caused by a low molecular weight of the P2VP block and consequently weak microphase separation in the melt is responsible for the formation of an alternating crystalline–amorphous lamellar phase. Additionally, our work presents for the first time the study of the influence of morphological characteristics of block copolymers on the ferroelectric properties (coercive field, remanent polarization, and maximum polarization) of P(VDF-TrFE)-based materials.

■ EXPERIMENTAL SECTION

Materials. 2-Vinylpyridine (2VP, Sigma-Aldrich, 97%) was dried overnight over CaH$_2$ and distilled under reduced pressure. 2,2′-Azobis(2-methylpropionitrile) (AIBN, Fluka, 98+%) was recrystallized twice from methanol, whereas copper(I) bromide (Sigma-Aldrich, 98%) was stirred for 1 h in glacial acetic acid and then filtered and washed with ethanol and diethyl ether before drying under vacuum. The chain transfer agent, 2-(dodecylthiocarbonothioylthio)-2-methylpropionic acid 3-azido-1-propanol ester (DDMAT-azide), was prepared according to the literature procedure.[37] The alkyne-

terminated initiator, 4-((trimethylsilyl)ethynyl)benzoyl peroxide, was prepared following a previous literature method.[38] Vinylidene fluoride (VDF, Synquest Laboratories, 98%), trifluoroethylene (TrFE, Synquest Laboratories, 98%), oxalyl chloride (Acros, 98%), 4-((trimethylsilyl)ethynyl)benzoic acid (Sigma-Aldrich), lithium peroxide (Li$_2$O$_2$, Acros, 95%), 1,1,4,7,7-pentamethyldiethylenetriamine (PMDETA, Acros, 99+%), 3-bromo-1-propanol (Acros, 97%), sodium azide (Sigma-Aldrich, >99.5%), *N*,*N*-dimethylformamide (DMF, Acros Organics, anhydrous, 99.8%), and dichloromethane (DCM, Acros Organics, anhydrous, ≥99.8%) were used as received. All other solvents were analytical grade.
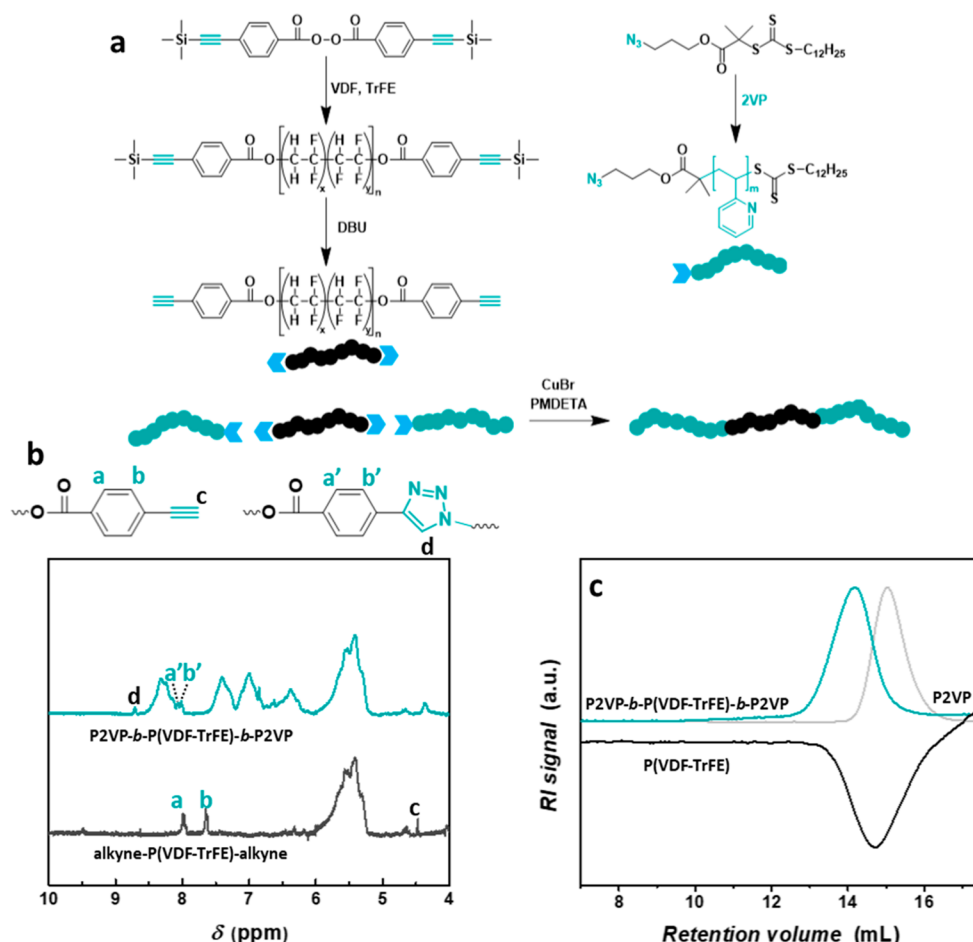
Synthesis of Alkyne-Terminated PVDF. 300 mL of 4-((trimethylsilyl)ethynyl)benzoyl peroxide (0.5 g, 1.15 mmol) solution in an anhydrous acetonitrile was introduced into a Parr (model 4568) high-pressure reactor and purged with N$_2$ to completely remove oxygen from the system. Subsequently, 3.5 bar of TrFE and 18 bar of VDF were transferred in the reactor, followed by an increase of the temperature to 90 °C. The reaction was allowed to proceed for 4 h under constant stirring. The reaction was stopped by fast cooling to room temperature and depressurization of the reaction mixture to remove unreacted monomers. The solvent was removed *in vacuo*, and the obtained solid was precipitated from DMF in MeOH:water (1:1) and washed twice with methanol and multiple times with chloroform to remove the initiator residues. The polymer was finally dried *in vacuo* at 45 °C to obtain light-yellow product. Note: higher molecular weight P(VDF-TrFE) used for block copolymers' synthesis with crystallization-driven self-assembly and lamellar morphology for D–E loop measurement was prepared by reducing the amount of the initiator (0.1 g, 0.23 mmol) (M_n = 22.5 kg mol^{-1}, Đ = 1.45, 30 mol % TrFE), whereas the pristine P(VDF-TrFE) used for ferroelectric measurement was synthesized using 0.05 g of the initiator (M_n = 28.1 kg mol^{-1}, Đ = 1.45, 30 mol % TrFE).

To a solution of (TMS-alkyne)-terminated P(VDF-TrFE) (2 g, 0.16 mmol) in 200 mL of a mixture acetonitrile:water (19:1), a slight excess of DBU (49.8 μL, 0.33 mmol) was added. The reaction mixture was allowed to stir for 2 h at 60 °C. Subsequently, the solvents were removed under vacuum, and the polymer was precipitated from DMF in a mixture of MeOH:water (1:1). The collected polymer was washed with MeOH and DCM and dried *in vacuo* at room temperature to yield a light-brown polymer.

Synthesis of Alkyne-Terminated P2VP. The monomer 2-vinylpyridine (5 mL, 84 mmol), chain transfer agent (DDMAT-azide) and AIBN were dissolved in anhydrous DMF and placed in a predried Schlenk tube. The reaction mixture was degassed via at least three freeze–pump–thaw cycles and placed in an oil bath at 70 °C. After reaction completion, DMF was removed and the THF solution was precipitated in a large excess of *n*-hexane. The precipitation procedure was repeated two times to fully remove unreacted species. The obtained light orange powder was dried under vacuum at room temperature for 1 day. The reaction conditions and the molecular characteristics of prepared polymers are listed in Table S1.

Synthesis of Block Copolymers. The alkyne-terminated P(VDF-TrFE) (300 mg, 0.029 mmol) and 1.3 mol equiv of P2VP to end groups of P(VDF-TrFE) were added into dried Schlenk tube. Subsequently, copper(I) bromide (4 equiv) was introduced, followed by the degassing of Schlenk tube. Polymers and metal catalyst were dissolved in 4 mL of anhydrous DMF, and 30 μL of PMDETA was added. The reaction was stirred for 4 days at 60 °C and afterward terminated. The reaction mixture was filtered twice using a neutral alumina column to remove the copper catalyst. The solution was concentrated and precipitated from THF in a 20-fold excess of hexane. The unreacted P2VP was removed by washing with methanol, and the final off-white product with typical yields of ca. 200–300 mg was obtained after precipitation of purified product from THF in hexane and subsequent drying at 45 °C.

Polymer Film Preparation. The polymers were dissolved in 4 mL of DMF (~10 mg/mL) and after passing through a 0.45 μm PTFE filter casted in an aluminum pan (ϕ 3 cm) at 45 °C. The obtained films were heated to 170 °C and kept isothermal for a few minutes to induce microphase separation. After fast cooling under

Figure 1. (a) Schematic representation of the synthesis of P(VDF-TrFE)-based block copolymers using CuAAc click coupling of alkyne-terminated P(VDF-TrFE) and azide-terminated P2VP. (b) Enlarged ^{1}H NMR spectra demonstrate the disappearance of the terminal alkyne signal **d** and shift of phenyl protons next to alkyne group to higher ppm values (peak **b**). The broad signal around 5.5 ppm corresponds to the TrFE units of P(VDF-TrFE). (c) GPC of P(VDF-TrFE) and the corresponding block copolymer indicate the successful preparation of block copolymers free of homopolymer contaminations.

ambient air, ∼20 μm thick free-standing films were obtained using the water lift-off method. All samples were dried overnight under vacuum at 60 °C.

Characterization. Nuclear magnetic resonance spectroscopy (^{1}H NMR) spectra were recorded on a 400 MHz Varian (VXR) spectrometer at room temperature. The molecular weights and dispersity of P(VDF-TrFE) and its block copolymers were measured by gel permeation chromatography (GPC) using THF as an eluent and triple detection, consisting of a Viscotek RALLS detector, a Viscotek viscometer model H502, and a Schambeck RI2012 refractive index detector. The separation was performed by utilizing two PLgel 5 μm MIXED-C, 300 mm columns from Agilent Technologies at 35 °C calibrated with narrow disperse polystyrene standards (Agilent Technologies and Polymer Laboratories). A predetermined refractive index (dn/dc) of 0.167 mL g^{-1} was used for calculation of the molecular weight of P2VP. Differential scanning calorimetry (DSC) thermograms were recorded on a TA Instruments DSC Q1000 by heating the sample to 170 °C and subsequently cooling to room temperature at 10 °C min^{-1}. Small-angle X-ray scattering (SAXS) and wide-angle X-ray scattering (WAXS) measurements were performed at the Dutch-Belgium Beamline (DUBBLE) station BM26B of the European Synchrotron Radiation Facility (ESRF) in Grenoble, France, strongly optimized for polymers.[39−41] SAXS images were recorded using a Pilatus 1M detector located 3.5 m away from the sample, while a Pilatus 300 KW dectector located 28 cm away from the sample was used for WAXS. The scattering 2θ angle scale was calibrated using the position of diffraction rings from a known silver

behenate standard sample. The scattering intensity curves are reported as a function of the modules of the scattering vector q, defined as $q = 4\pi/\lambda(\sin \theta)$ with 2θ being the scattering angle and λ the wavelength of the X-rays (0.97 Å). Some of the X-ray measurements were also conducted at the MINA beamline in Groningen on a diffractometer equipped with Cu rotating anode (λ = 1.5413 Å). The sample-to-detector distance at MINA was 3 m, and the SAXS images were collected using a Bruker Vantec2000 detector. Transmission electron microscopy (TEM) was performed on a Philips CM12 transmission electron microscope operating at an accelerating voltage of 120 kV. A piece of the block copolymer film was embedded in epoxy resin and microtomed using a Leica Ultracut UCT-ultramicrotome to prepare ultrathin sections (ca. 80 nm). No additional staining of the samples was performed.

Hysteresis Loop Measurements. The $D−E$ hysteresis measurements were performed using a state-of-the-art ferroelectric−piezoelectric tester aixACCT equipped with a Piezo Sample Holder Unit with a high-voltage amplifier (0−10 kV). An ac electric field with a triangular waveform at a frequency of 10 Hz was applied over polymer films immersed in silicon oil. The field was gradually increased up to 250 MV m^{-1}. 100 nm thick gold electrodes (ca. 3.14 mm^2) with 5 nm chromium adhesion layer were evaporated onto both sides.

■ RESULTS AND DISCUSSION

A facile approach for the synthesis of P2VP-b-P(VDF-TrFE)-b-P2VP triblock copolymers that combines free radical copolymerization of VDF and TrFE and reversible addition−

fragmentation chain transfer (RAFT) polymerization of 2VP and their subsequent combination via click reaction is introduced here (Figure 1). The free radical copolymerization of VDF and TrFE monomers is conducted using 4-((trimethylsilyl)ethynyl)benzoyl peroxide as an initiator in acetonitrile at 90 °C.[38] Because the radical polymerization of fluorinated monomers occurs exclusively through the combination of radicals,[42] and chain transfer reactions to acetonitrile are negligible, the alkyne functional groups of the initiator are almost exclusively incorporated at both chain ends of the copolymer. The protecting trimethylsilyl (TMS) groups are quantitatively removed with DBU in an acetonitrile:water (19:1) mixture (Figure S1). The molar content of TrFE units inside the copolymer, determined via ^{1}H NMR spectroscopy, is 25%, while the number-average molecular weight and dispersity index calculated from gel permeation chromatography (GPC) are 10500 g mol^{-1} and 1.51, respectively. Azide-terminated P2VP is produced via RAFT using a functionalized chain transfer agent (DDMAT-azide). P2VP is a desirable amorphous block, not only because of its glass transition temperature that is high enough to prevent breakout crystallization from an ordered melt but also due to its hydrogen bonding potential, allowing the possibility to selectively incorporate various nanoobjects and functional molecules inside block copolymers.[43,44] To prepare block copolymers with different ratios between the blocks, several different azide-terminated P2VPs are synthesized by changing the reaction times and the chain transfer agent to monomer ratio (Table S1).

Block copolymers are synthesized using copper(I)-catalyzed azide−alkyne cycloaddition (CuAAc) reaction of telechelic P(VDF-TrFE) and P2VP in the presence of a copper(I) bromide−$N,N,N'N'',N''$-pentamethyldiethylenetriamine (PMDETA) complex at 60 °C. To ensure the complete conversion of P(VDF-TrFE) alkyne end-groups, P2VP is added in excess (1.3 equiv). The excess of P2VP is subsequently washed away with methanol, a selective solvent for P2VP. The completion of the reaction and the successful preparation of block copolymers are determined using ^{1}H NMR spectroscopy by the disappearance of the signal from terminal alkyne protons and a shift of the signal corresponding to the phenyl protons next to the alkyne group. Additionally, a clear change of the GPC signal toward a lower retention volume is observed after the click reaction and P2VP removal. Importantly, no additional signals of the homopolymers are detectable, which confirms the successful synthesis of pure block copolymers. Four different block copolymers, titled BCP1, BCP2, BCP3, and BCP4, with different P(VDF-TrFE) content are synthesized, and their molecular characteristics are listed in Table 1. The P(VDF-TrFE) content decreases going from BCP1 to BCP4.

Block copolymer films are prepared using solvent casting from DMF, followed by thermal annealing at 170 °C for a few minutes and cooling to ambient temperature to induce crystallization of P(VDF-TrFE). Short annealing times are found to be enough to reach the equilibrium structure, probably due to the low molecular weight and high mobility of the block copolymer melt. The phase behavior of block copolymer samples is investigated using small-angle X-ray scattering (SAXS) in the melt and at room temperature and also using transmission electron microscopy (TEM) as complementary technique, after crystallization of P(VDF-TrFE).[39,40] At high P(VDF-TrFE) content (BCP1), a

**Table 1. Characteristics of the Polymers Used for Self-Assembly Study**

polymer name	M_n (kg mol^{-1})	Đ	$f_{P(VDF-TrFE)}$[c] (wt %)	$\Phi_{P(VDF-TrFE)}$[c] (vol %)
P(VDF-TrFE)	10.5[a]	1.51	100	100
BCP1	11.6[b]	1.83	90.5	85
BCP2	15.3[b]	1.79	69	57
BCP3	19.1[b]	1.81	55	42
BCP4	27.6[b]	1.63	38	27
P(VDF-TrFE)a	28.1[a]	1.45	100	100
BCP1a	25.0[b]	1.85	90.5	85
BCP2a	32.8[b]	1.80	70	58

[a]Determined using GPC. [b]Molecular weight calculated from $M_{n,GPC}$ values of P(VDF-TrFE) taking into account the ratio between the blocks calculated using ^{1}H NMR. [c]Weight fraction of P(VDF-TrFE) determined using ^{1}H NMR as described in the Supporting Information. [d]The volume fractions were calculated using the weight fractions and the density of P2VP (1.14 g cm^{-3}) and P(VDF-TrFE) (1.88 g cm^{-3}).

disordered melt structure is observed, mainly due to the low molecular weight of the block copolymer and hence a low χN value. The SAXS scattering profile at 170 °C is characterized by a single broad peak, arising from a correlation hole effect formed due to concentration fluctuations in the melt (Figure 2a).[45] However, upon crystallization, a new scattering peak appears with maximum located at lower scattering angles $q* = 0.21$ nm^{-1}, indicating that the P(VDF-TrFE) crystallization drives the formation of an alternating P(VDF-TrFE) crystalline-(P(VDF-TrFE) + P2VP) amorphous lamellar structure. The lack of high order peaks suggests short-range ordering of the structure as confirmed also by TEM (Figure 3a). Similar behavior was already observed in the P2VP-*b*-PVDF-*b*-P2VP and PLLA-*b*-PVDF-*b*-PLLA and many other crystalline−amorphous block copolymer systems with a crystalline block as the major component.[15,29,35,46]

In contrast to the BCP1, the block copolymers with higher content of P2VP demonstrate a good phase separation in the molten state. The SAXS profile of BCP2 reveals a clear lamellar morphology in the melt, distinguished by two strong signals with a ratio $1q*:2q*$ where the main peak centered around $q* = 0.29$ nm^{-1} corresponds to the lamellar spacing $d = 2\pi/q* = 21.5$ nm (Figure 2b). Upon cooling, crystallization of P(VDF-TrFE) is confined inside the lamellar domains formed in the melt as a result of the self-assembly of block copolymers. The TEM image of the block copolymer after crystallization (Figure 3b), together with no significant changes in the SAXS profile (Figure 3c), supports the existence of lamellar microdomains and crystallization confinement. Moreover, the lamellar domain spacing measured by TEM is similar to the value obtained from SAXS. It is also important to note that the contrast between the phases in TEM images is a consequence of the density difference between crystalline and amorphous blocks. Therefore, dark layers correspond to the crystalline P(VDF-TrFE), while P2VP layers appear lighter in the TEM images.

When the volume fraction of the P2VP is increased to 0.58, the SAXS profile of the BCP3 in the melt shows a main scattering peak at $q* = 0.24$ nm^{-1} and a number of higher order reflections with position of $\sqrt{3}q*$ and $\sqrt{4}q*$ characteristic for hexagonally packed P(VDF-TrFE) cylinders ($d_{cyl} \approx 19$ nm) inside the P2VP matrix (Figure 2c). As expected, the cylindrical structure is retained after cooling and confined
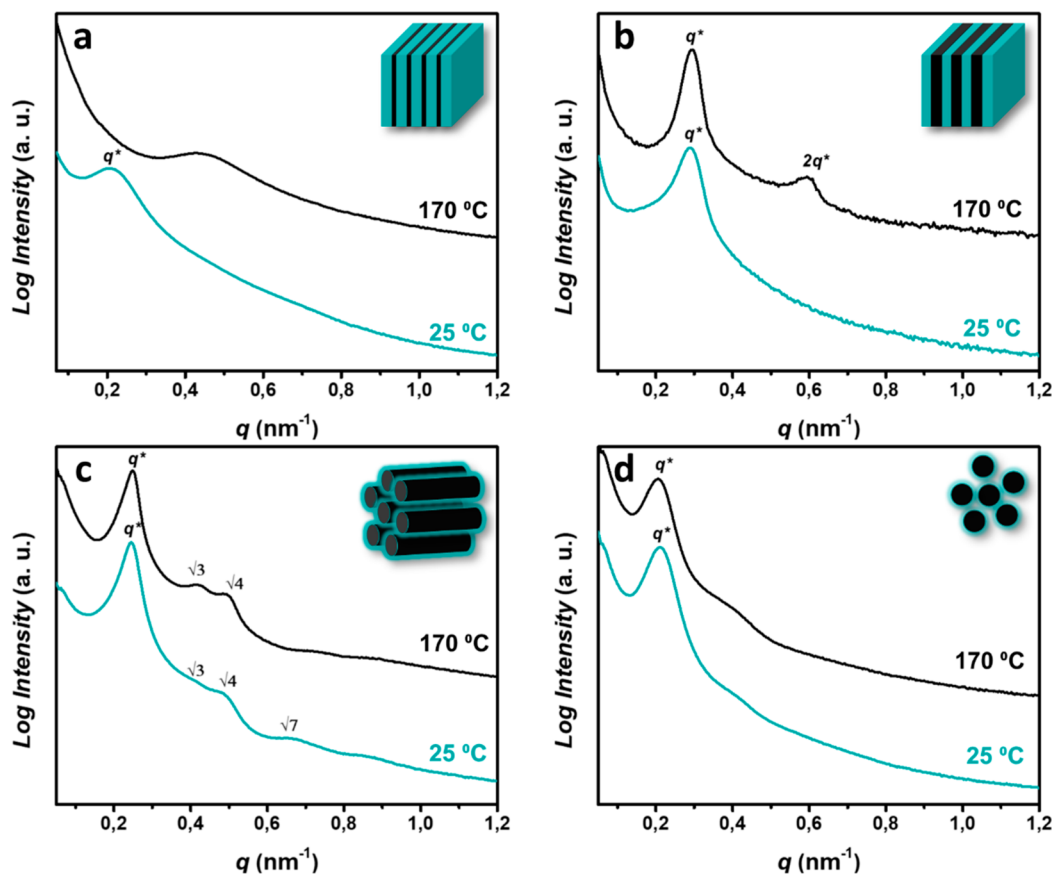
Figure 2. (a) SAXS profile for BCP1 collected at 170 °C and at room temperature showing the formation of a disordered melt and a crystallization-driven self-assembly upon cooling to room temperature. Unlike this block copolymer, in BCP2, BCP3, and BCP4 crystallization is confined inside (b) lamellar, (c) cylindrical, and (d) spherical nanodomains, respectively.
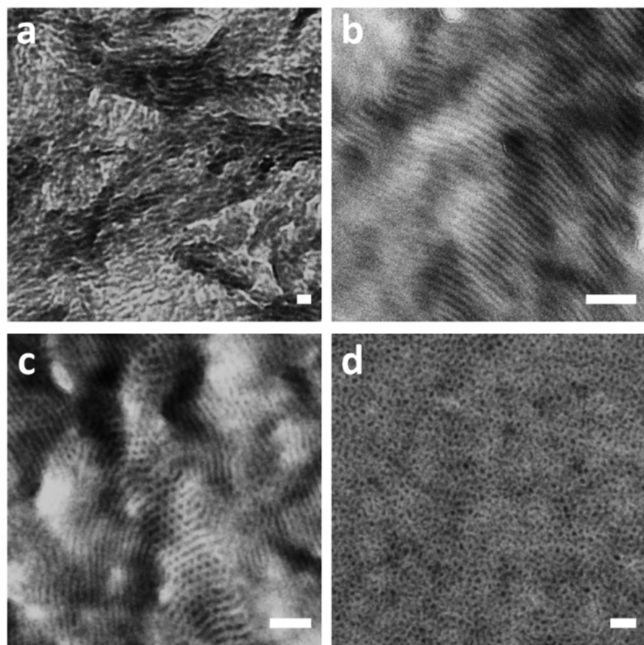
Figure 3. TEM micrographs of block copolymers indicating (a) crystallization induced lamellar structure, (b) lamellar, (c) cylindrical, and (d) disordered spherical structure obtained after a crystallization inside the domains formed via self-assembly of the block copolymers in the melt. All samples were annealed for 5 min in the melt and cooled using ambient air. The scale bars correspond to 100 nm.

crystallization of P(VDF-TrFE). The information about the morphology obtained with SAXS is consistent with the TEM image of the block copolymer, which shows both parallelly and perpendicularly oriented cylindrical domains (Figure 3c). The cylindrical morphology is for the first time observed for PVDF-based block copolymers. In a similar system, P2VP-*b*-PVDF-*b*-P2VP, no cylindrical structure is detected at the same molecular weights and the same ratio of the blocks.[36] The probable reason for this dissimilarity lays in the fact that incorporation of the TrFE inside the block copolymer increases the fluorine content in the polymer backbone, causing stronger immiscibility of the two blocks and thus increased segregation strength.

Finally, we examine the morphological features of BCP4 with only 27 vol % P(VDF-TrFE). The SAXS profile at 170 °C shows only one strong scattering peak at $q^* = 0.20$ nm^{-1} together with a second weak oscillation (Figure 2d). Again, the shape of the SAXS profile is preserved upon the confined crystallization of P(VDF-TrFE). TEM shows the existence of disordered spherically shaped micellar morphology, where P(VDF-TrFE) crystalline micelles are embedded inside the amorphous P2VP matrix (Figure 3d). Similarly disordered micellar structures are found in various sphere-forming semicrystalline block copolymers.[15,47]

The composition at which the order−order (LAM-CYL and CYL-SPH) phase boundaries are observed is somewhat shifted compared to the symmetric phase diagram. Bearing in mind that the dispersity of the middle P(VDF-TrFE) block is relatively high ($Đ = 1.51$), such a difference may be attributed

to the effect of dispersity on self-assembly. It has been recently observed that a lamellar composition window in ABA block copolymers with a disperse B block is shifted to higher volume fractions of the B block compared to monodisperse analogues, favoring the formation of a morphology with larger interfacial curvature.[20,48]

The crystallization mechanism inside block copolymers and the influence of the self-assembled morphology on the crystal formation are evaluated using differential scanning calorimetry (DSC). Samples annealed at 170 °C for 5 min are cooled at a rate of 10 °C min^{-1}, and the respective cooling scans are given in Figure 4. The DSC thermogram of pure P(VDF-TrFE)
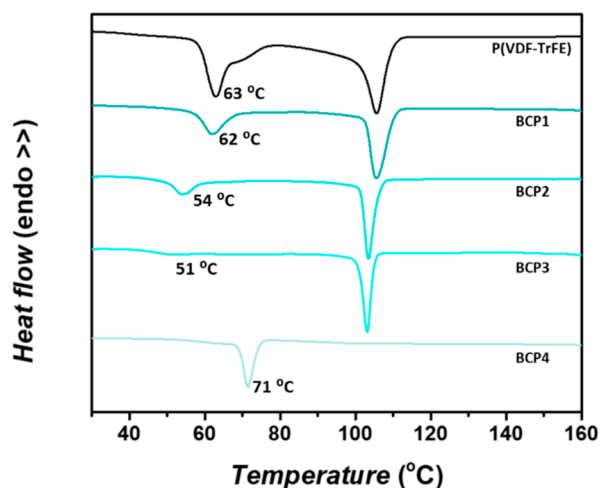

Figure 4. DSC cooling curves for pristine P(VDF-TrFE) and its block copolymers indicating strong influence of the morphology on the crystallization mechanism and degree of crystallinity.

displays two exothermic signals: a crystallization peak at T_c = 105 °C and a second peak corresponding to a paraelectric−ferroelectric Curie transition at T_{Curie} = 63 °C. No significant change in the crystallization temperature compared to P(VDF-TrFE) is observed for BCP1, BCP2, and BCP3, whereas BCP4 with a spherical morphology demonstrates a considerable drop in the crystallization temperature (ΔT = 34 °C). This indicates that different mechanisms are responsible for the formation of crystals in lamellar and cylindrical block copolymers compared to the crystallization inside spherical nanodomains. Impurities present in BCP1, BCP2, and BCP3 act as crystallization nuclei that promote heterogeneous nucleation characterized by no significant undercooling and long-range crystal growth. In contrast, small isolated spherical domains largely exceed the number of impurities, which leads to a homogeneous nucleation of the crystals and to a serious drop of the crystallization temperature.[25,28,47]

Besides crystallization, the paraelectric−ferroelectric phase transition, accompanied by conformational changes inside the crystals, shows clear dependency on the type of the block copolymer morphology. While BCP1 does not show a significant change in the Curie temperature compared to the P(VDF-TrFE) homopolymer, a strong reduction is demonstrated for the block copolymers BCP2 and BCP3, where confined crystallization takes place inside lamellar or cylindrical domains. A much lower Curie temperature has already been demonstrated for ultrathin Langmuir−Blodgett P(VDF-TrFE) films and in nanowires formed inside of 15 nm diameter pores of an aluminum oxide membrane.[50,51] In both cases the

reduction of the Curie temperature has been ascribed to the polymer in contact with surface layers. The decrease of the Curie temperature can additionally be the consequence of the confinement effect related to domain size reduction. The drop of the Curie transition is also followed by a decrease in the phase transition enthalpy values. This reduction cannot just be explained by dilution effects of P2VP, but it is mainly due to the reduction of the domain size caused by the confinement of the crystallization inside nanodomains. It is worth noting that a stronger reduction of the Curie temperature and enthalpy of this phase transition are detected for the cylindrical morphology, probably due to a stronger spatial confinement and a larger contact surface with the P2VP. Interestingly, an immediate crystallization into the ferroelectric phase directly from the melt is demonstrated for BCP4 having a spherical morphology, where no Curie transition is observed. This is furthermore confirmed by using temperature-resolved wide-angle X-ray scattering (WAXS), where no peak characteristic for the paraelectric phase is observed during crystallization (Figure S2). Similar findings have been reported for a P2VP-*b*-PVDF-*b*-P2VP block copolymer, where confined crystallization inside spherical domains leads to the crystallization of PVDF into the ferroelectric β-phase, which has been associated with the fact that maximum of the crystallization rate for β-phase coincides with the reduced crystallization temperature caused by the homogeneous nucleation.[36]

The preservation of the P(VDF-TrFE) crystalline structure in the ferroelectric phase is of crucial importance for the application of these block copolymers in devices. Therefore, the crystalline nature of the block copolymers is further confirmed by WAXS. In all samples, the scattering peak at q = 14.1 nm^{-1} corresponds to the reflections in the (110) and (200) planes of the P(VDF-TrFE) low-temperature ferroelectric phase (LTFE) with *all-trans* conformation (Figure 5).[3]
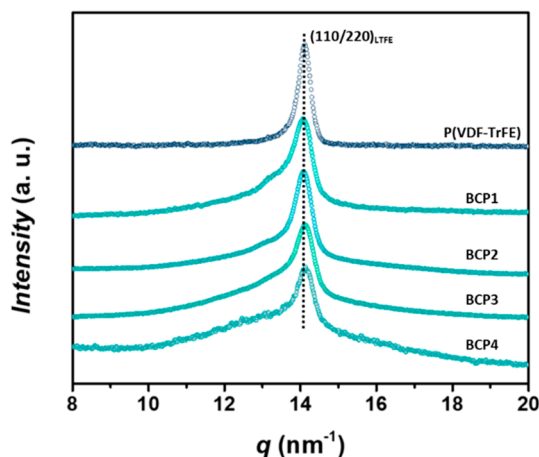
Figure 5. WAXS profiles for (PVDF-TrFE) and its block copolymers at room temperature. The (110/220) peak corresponds to a low-temperature ferroelectric phase and is present in all block copolymers. All block copolymers show preservation of the ferroelectric crystalline phase with high crystallinity.

Compared to polymers in which the crystallization occurs via heterogeneous nucleation mechanism, a large amorphous halo of the P2VP block and a less pronounced crystalline peak appear for the block copolymer with spherical morphology. This is not surprising since the crystallization is confined in all three dimensions. This is in contrast to the lamellar and

cylindrical morphologies where the fast crystal propagation is possible in at least one dimension. The degree of crystallinity (χ_c) of P(VDF-TrFE) inside block copolymers is calculated from the enthalpy of crystallization, and the values are listed in Table 2. Because ferroelectric properties of a material are

Table 2. Crystallization Properties of P(VDF-TrFE) and Its Block Copolymers

polymer name	$T_c{}^a$ (°C)	$T_{Curie}{}^a$ (°C)	ΔH_c (J g^{-1})	ΔH_{Curie} (J g^{-1})	$X_c{}^b$ (%)	$X_c{}^c$ (%)
P(VDF-TrFE)	105	63	16.8	8.0	40.0	40.0
BCP1	105	62	13.9	6.7	33.1	36.5
BCP2	103	54	11.5	2.9	27.4	39.7
BCP3	103	51	8.0	0.8	19.1	34.7
BCP4	71	n.a.	6.5	n.a.	7.4	19.5

^{a}Determined from DSC thermograms. ^{b}Overall crystallinity calculated using the following equation: $X_c = (\Delta H_c / \Delta H_{100}) \times 100\%$. ΔH_c was determined based on DSC thermograms. $\Delta H_{100} = 42$ J g^{-1} for crystallization in the paraelectric phase.[49] The heat of fusion for crystallization in the ferroelectric phase, such as in the case of BCP4, is unknown. However, the assumed value is 2.1 times higher than that for a paraelectric phase as observed for pure PVDF.[36] ^{c}True crystallinity values after normalization to the P(VDF-TrFE) weight percentage.

dependent on the overall crystallinity and not the crystallinity with respect to the ferroelectric component only, the addition of P2VP side chains leads to a decrease of crystallinity due to the dilution of crystals with an amorphous component. However, if we consider the dilution effect of the P2VP, no drastic change of the crystallinity compared to the parent P(VDF-TrFE) is observed for all samples except the BCP4, demonstrating that the introduction of P2VP and its phase separation from P(VDF-TrFE) in lamellar or cylindrical morphology do not impede the crystallization of P(VDF-TrFE). In contrast to this, in some other block copolymer systems considerable disruption of the crystallization is observed after confinement inside nanodomains.[47] However, as already demonstrated by WAXS, constrained crystallization inside spherical domains (BCP4) leads to a significant reduction in crystallinity compared to the parent P(VDF-TrFE).

Ferroelectric properties of the block copolymers are examined in detail by $D-E$ loop measurements where a bipolar triangular waveform is applied at a frequency of 10 Hz up to an electric field of 250 MV m^{-1}. The molecular weight of pristine P(VDF-TrFE) and BCP1 was not high enough to provide good film formation and satisfying breakdown strength. Thus, new polymers, P(VDF-TrFE)a and BCP1a, with higher molecular weights but identical molecular and morphological characteristics were synthesized (Figure S3). Moreover, since a mismatch exists between the thickness of the lamellar layer in BCP2 and the diameter of cylinders in BCP3, we prepared a new block copolymer, BCP2a, with lamellar morphology and the lamella thickness corresponding to the diameter of the cylinders in BCP3. Figure 6 demonstrates a strong effect of the amorphous P2VP content and the morphology type on the ferroelectric response of the block copolymers. The switching of the dipoles, demonstrated by a peak appearance on the current−electric field ($I-E$) diagram and the rectangular shape of the hysteresis loop, is observed for the pristine polymer and block copolymers BCP1a and BCP2a.

Additionally, a slight decrease in the coercive field for BCP1a and an increase for BCP2a are obtained compared to the pristine P(VDF-TrFE). Note that the maximum and remanent polarization for all samples show a decrease with respect to P(VDF-TrFE) due to the incorporation of the nonferroelectric amorphous P2VP with a dielectric constant lower than amorphous P(VDF-TrFE).

The dipole flipping inside ferroelectric materials containing an additional nonferroelectric component is mostly affected by the distribution of the electric field inside material, the size of the ferroelectric domains, and coupling forces between them.[52−55] Incorporation of the lower dielectric constant P2VP results in an uneven distribution of electric fields inside the nanodomains. Consequently, the crystalline (PVDF-TrFE) domains in all block copolymers sense a lower nominal electric field than applied, and therefore the dipole alignment and chain rotation should take place at higher fields compared to the pristine P(VDF-TrFE).[56] Nevertheless, the addition of an amorphous component reduces the number of adjacent ferroelectric domains and increases the distance between them, which results in a reduction of the coupling forces and an easier switching of the crystalline dipoles. Therefore, the values of the coercive field, associated with the energy required for the dipole reversal, are caused by these two effects which have opposite action directions. In BCP1 the amount of amorphous relatively polar P2VP is too small to cause a drastic change in the dielectric constant of the amorphous phase or a large discrepancy between the local and the applied electric field. This, together with a weakened coupling influenced by the incorporation of insulating segments, is the main cause for the modest reduction of the coercive field compared to the neat P(VDF-TrFE). The same reasoning stands behind the slightly elevated coercive field for BCP2, where a stronger reduction of the local electric field in crystalline lamellae shifts the coercive field to higher values.

In contrast to block copolymers with a lamellar morphology produced by either crystallization-driven self-assembly or confined crystallization from the phase separated melt, block copolymers BCP3 and BCP4 with P(VDF-TrFE) crystals formed inside cylindrical and spherical domains did not demonstrate dipole switching up to 250 M m^{-1} at a frequency of 10 Hz (Figure 6). However, the reduction of the frequency to 1 Hz, granting more time for dipoles to align, allows the dipole switching and loop opening for BCP3 at a field as high as 250 MV m^{-1} (Figure S4). It is important to note that the block copolymers BCP3 and BCP4 with P2VP as major component display considerable conductive losses probably related to the copper ion impurities not completely removed after the synthesis mostly present in P2VP phase.[57] A strong delay of the loop opening for BCP3 or unobservable ferroelectricity for BCP4 cannot be explained exclusively by the reduction of the dielectric constant of the amorphous phase and uneven distribution of the electric field between phases. As already deduced after comparing the values of Curie transition and enthalpy values for this phase transition, the crystalline domain size inside cylinders is reduced compared to the block copolymer with lamellar morphology. Additionally, decreased chain mobility is demonstrated for the crystalline phase inside cylindrical domains due to substantial surface effects of the P2VP. When the crystal size is small, the coupling among ferroelectric domains is weak, and thus a high field is necessary to induce the growth of ferroelectric domains to a size where dipoles will stay aligned after the removal of the
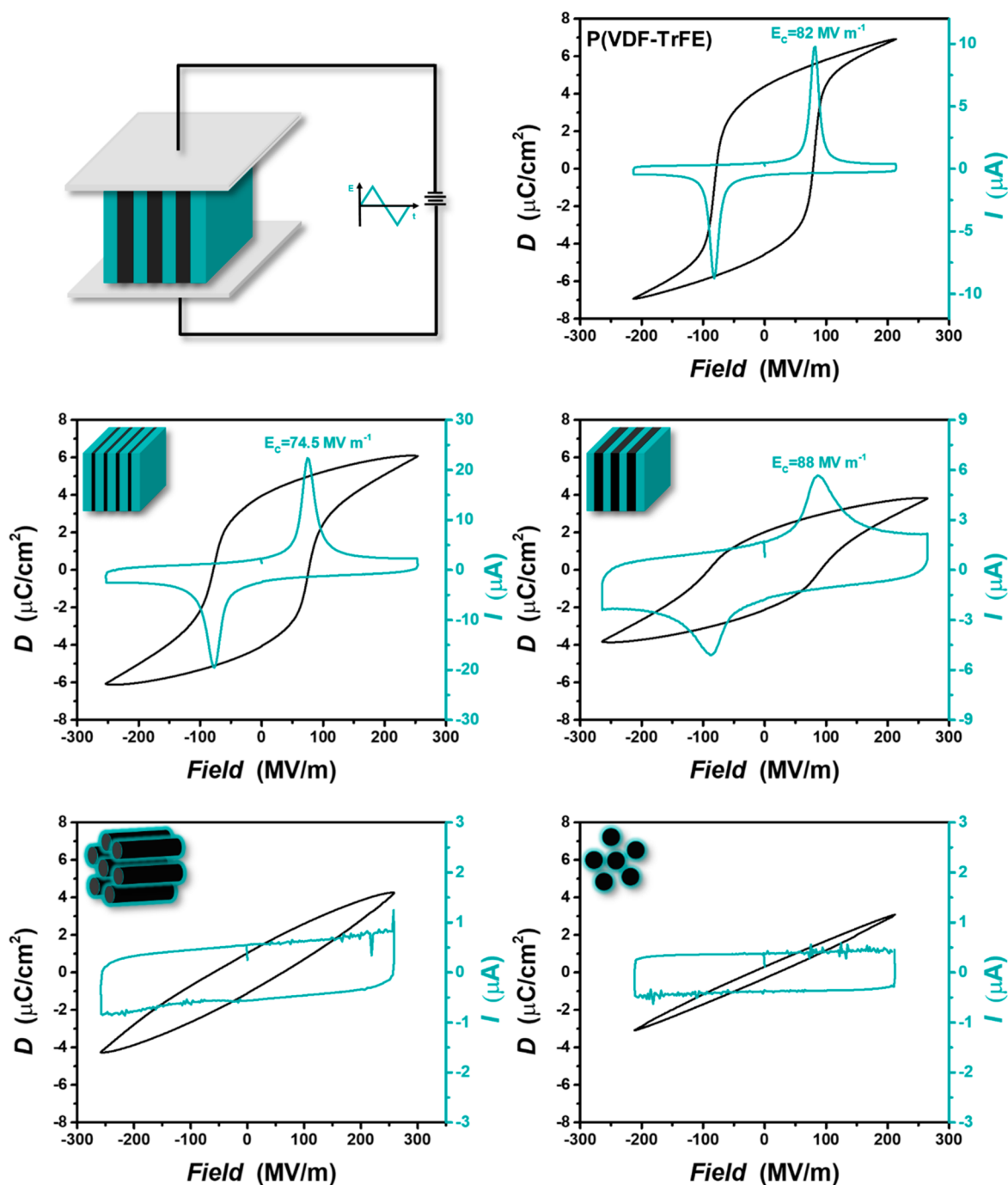
Figure 6. Structure−ferroelectric response relationship of the block copolymers. Ferroelectric properties of block copolymers are examined by $D-E$ and $I-E$ measurements using a bipolar triangular waveform 10 Hz at an electric field around 250 MV m^{-1}.

field. In addition, the reduced mobility of polymer chains increases the energy needed for the chain rotation, and therefore dipole switching is delayed compared to the lamellar block copolymer. It is expected that the confinement of P(VDF-TrFE) inside spherical domains shifts the dipole flipping to even higher fields or that the ferroelectric behavior of this block copolymer will be completely absent since the growth of ferroelectric domains is spatially restricted in small isolated nanodomains, which is not the case for samples with one- or two-dimensional confinement. Unfortunately, this remains hypothetical since the molecular weight and break-down strength of BCP4 are not sufficient enough to reach the

electric fields of interest. Nevertheless, the reduced cooperative ferroelectricity caused by confining the crystallization inside cylindrical or spherical domains of block copolymers, although not valuable for memory storage applications, is of potential for electrical energy storage where no or delayed polarization saturation and low ferroelectric losses are highly desired.[58,59]

■ CONCLUSION

In summary, we developed a simple method for preparing ferroelectric nanostructures by confining crystallization inside nanodomains produced by the self-assembly of P2VP-*b*-P(VDF-TrFE)-*b*-P2VP block copolymers. Different morphol-

ogies, such as lamellar, hexagonally packed cylinders, and spherical, are easily achieved by simply changing the ratio between blocks. The type of morphology influences the overall crystallinity and crystalline domain size. While the crystallization temperature and the degree of crystallinity for the lamellar and cylindrical block copolymers are not significantly altered by the confinement, the significant drop of the crystallization temperature and crystallinity are observed for block copolymers with spherical structure due to homogeneous nucleation inside isolated spherical domains. In addition, with increasing the confinement level, the crystalline domains reduce in size, seriously influencing the ferroelectric response of the block copolymers. The dipole flipping inside the block copolymers is shown to be affected by the size of the ferroelectric domains and coupling forces between them and the distribution of the nominal electric field inside material. Samples with lamellar morphology, obtained either from the crystallization-driven self-assembly or after confinement in lamellar morphology obtained in the melt, demonstrate ferroelectric switching at fields similar to the pristine P(VDF-TrFE), whereas delayed polarization saturation or linear dielectric behavior is demonstrated for block copolymers with isolated cylindrical and spherical nanostructures. This work offers a promising way for preparing P(VDF-TrFE) nanostructures and, additionally, for tuning their response to an electric field.

ASSOCIATED CONTENT

Ⓢ Supporting Information

The Supporting Information is available free of charge on the ACS Publications website at DOI: 10.1021/acs.macromol.8b02131.

> ^{1}H NMR spectra of TMS-protected and alkyne-terminated P(VDF-TrFE), temperature-resolved WAXS of neat P(VDF-TrFE) and BCP4, SAXS profiles and DSC thermograms of the block copolymers with higher molecular weight, $D-E$ and $I-E$ results for BCP3 at 1 Hz (PDF)

AUTHOR INFORMATION

Corresponding Author

*E-mail k.u.loos@rug.nl; Tel +31-50 363 6867.

ORCID Ⓞ

Giuseppe Portale: 0000-0002-4903-3159

Katja Loos: 0000-0002-4613-1159

Notes

The authors declare no competing financial interest.

REFERENCES

(1) Chen, X.; Han, X.; Shen, Q.-D. PVDF-Based Ferroelectric Polymers in Modern Flexible Electronics. *Adv. Electron. Mater.* **2017**, 3 (5), 1600460.

(2) Ameduri, B. From Vinylidene Fluoride (VDF) to the Applications of VDF-Containing Polymers and Copolymers: Recent Developments and Future Trends. *Chem. Rev.* **2009**, 109 (12), 6632–6686.

(3) Soulestin, T.; Ladmiral, V.; Dos Santos, F. D.; Améduri, B. Vinylidene Fluoride- and Trifluoroethylene-Containing Fluorinated Electroactive Copolymers. How Does Chemistry Impact Properties? *Prog. Polym. Sci.* **2017**, 72, 16–60.

(4) Hu, Z.; Tian, M.; Nysten, B.; Jonas, A. M. Regular Arrays of Highly Ordered Ferroelectric Polymer Nanostructures for Non-Volatile Low-Voltage Memories. *Nat. Mater.* **2009**, 8 (1), 62–67.

(5) Lee, J.-H.; Yoon, H.-J.; Kim, T. Y.; Gupta, M. K.; Lee, J. H.; Seung, W.; Ryu, H.; Kim, S.-W. Micropatterned P(VDF-TrFE) Film-Based Piezoelectric Nanogenerators for Highly Sensitive Self-Powered Pressure Sensors. *Adv. Funct. Mater.* **2015**, 25 (21), 3203–3209.

(6) Bae, S.-H.; Kahya, O.; Sharma, B. K.; Kwon, J.; Cho, H. J.; Özyilmaz, B.; Ahn, J.-H. Graphene-P(VDF-TrFE) Multilayer Film for Flexible Applications. *ACS Nano* **2013**, 7 (4), 3130–3138.

(7) Kang, S. J.; Bae, I.; Shin, Y. J.; Park, Y. J.; Huh, J.; Park, S.-M.; Kim, H.-C.; Park, C. Nonvolatile Polymer Memory with Nano-confinement of Ferroelectric Crystals. *Nano Lett.* **2011**, 11 (1), 138–144.

(8) Naber, R. C. G.; Tanase, C.; Blom, P. W. M.; Gelinck, G. H.; Marsman, A. W.; Touwslager, F. J.; Setayesh, S.; d eLeeuw, D. M. High-Performance Solution-Processed Polymer Ferroelectric Field-Effect Transistors. *Nat. Mater.* **2005**, 4 (3), 243–248.

(9) Yuan, Y.; Reece, T. J.; Sharma, P.; Poddar, S.; Ducharme, S.; Gruverman, A.; Yang, Y.; Huang, J. Efficiency Enhancement in Organic Solar Cells with Ferroelectric Polymers. *Nat. Mater.* **2011**, 10 (4), 296–302.

(10) Cauda, V.; Stassi, S.; Bejtka, K.; Canavese, G. Nanoconfinement: An Effective Way to Enhance PVDF Piezoelectric Properties. *ACS Appl. Mater. Interfaces* **2013**, 5 (13), 6430–6437.

(11) Kassa, H. G.; Cai, R.; Marrani, A.; Nysten, B.; Hu, Z.; Jonas, A. M. Structure and Ferroelectric Properties of Nanoimprinted Poly-(Vinylidene Fluoride-Ran-Trifluoroethylene). *Macromolecules* **2013**, 46 (21), 8569–8579.

(12) Liu, Y.; Weiss, D. N.; Li, J. Rapid Nanoimprinting and Excellent Piezoresponse of Polymeric Ferroelectric Nanostructures. *ACS Nano* **2010**, 4 (1), 83–90.

(13) García-Gutiérrez, M.-C.; Linares, A.; Martín-Fabiani, I.; Hernández, J. J.; Soccio, M.; Rueda, D. R.; Ezquerra, T. A.; Reynolds, M. Understanding Crystallization Features of P(VDF-TrFE) Copolymers under Confinement to Optimize Ferroelectricity in Nanostructures. *Nanoscale* **2013**, 5 (13), 6006–6012.

(14) Whiter, R. A.; Narayan, V.; Kar-Narayan, S. A Scalable Nanogenerator Based on Self-Poled Piezoelectric Polymer Nanowires with High Energy Conversion Efficiency. *Adv. Energy Mater.* **2014**, 4 (18), 1400519.

(15) Ho, V.; Boudouris, B. W.; McCulloch, B. L.; Shuttle, C. G.; Burkhardt, M.; Chabinyc, M. L.; Segalman, R. A. Poly(3-Alkylthiophene) Diblock Copolymers with Ordered Microstructures and Continuous Semiconducting Pathways. *J. Am. Chem. Soc.* **2011**, 133 (24), 9270–9273.

(16) Jin, X.-H.; Price, M. B.; Finnegan, J. R.; Boott, C. E.; Richter, J. M.; Rao, A.; Menke, S. M.; Friend, R. H.; Whittell, G. R.; Manners, I. Long-Range Exciton Transport in Conjugated Polymer Nanofibers Prepared by Seeded Growth. *Science* **2018**, 360 (6391), 897–900.

(17) Smart, T.; Lomas, H.; Massignani, M.; Flores-Merino, M. V.; Perez, L. R.; Battaglia, G. Block Copolymer Nanostructures. *Nano Today* **2008**, 3 (3), 38–46.

(18) Mai, Y.; Eisenberg, A. Self-Assembly of Block Copolymers. *Chem. Soc. Rev.* **2012**, 41 (18), 5969–5985.

(19) Hadjichristidis, N.; Iatrou, H.; Pitsikalis, M.; Pispas, S.; Avgeropoulos, A. Linear and Non-Linear Triblock Terpolymers.

Synthesis, Self-Assembly in Selective Solvents and in Bulk. *Prog. Polym. Sci.* **2005**, *30* (7), 725−782.

(20) Widin, J. M.; Schmitt, A. K.; Schmitt, A. L.; Im, K.; Mahanthappa, M. K. Unexpected Consequences of Block Polydispersity on the Self-Assembly of ABA Triblock Copolymers. *J. Am. Chem. Soc.* **2012**, *134* (8), 3834−3844.

(21) Park, J.; Lee, K. S.; Choi, C.; Kwak, J.; Moon, H. C.; Kim, J. K. Effect of Molecular Weight on Competitive Self-Assembly of Poly(3-Dodecylthiophene)-Block-Poly(Methyl Methacrylate) Copolymers. *Macromolecules* **2016**, *49* (9), 3647−3653.

(22) Angelescu, D. E.; Waller, J. H.; Adamson, D. H.; Deshpande, P.; Chou, S. Y.; Register, R. A.; Chaikin, P. M. Macroscopic Orientation of Block Copolymer Cylinders in Single-Layer Films by Shearing. *Adv. Mater.* **2004**, *16* (19), 1736−1740.

(23) Thurn-Albrecht, T.; DeRouchey, J.; Russell, T. P.; Kolb, R. Pathways toward Electric Field Induced Alignment of Block Copolymers. *Macromolecules* **2002**, *35* (21), 8106−8110.

(24) Rokhlenko, Y.; Gopinadhan, M.; Osuji, C. O.; Zhang, K.; O'Hern, C. S.; Larson, S. R.; Gopalan, P.; Majewski, P. W.; Yager, K. G. Magnetic Alignment of Block Copolymer Microdomains by Intrinsic Chain Anisotropy. *Phys. Rev. Lett.* **2015**, *115* (25), 258302.

(25) Michell, R. M.; Müller, A. J. Confined Crystallization of Polymeric Materials. *Prog. Polym. Sci.* **2016**, *54−55*, 183−213.

(26) He, W.-N.; Xu, J.-T. Crystallization Assisted Self-Assembly of Semicrystalline Block Copolymers. *Prog. Polym. Sci.* **2012**, *37* (10), 1350−1400.

(27) Voet, V. S. D.; Tichelaar, M.; Tanase, S.; Mittelmeijer-Hazeleger, M.; ten Brinke, G.; Loos, K. Poly(Vinylidene Fluoride)/Nickel Nanocomposites from Semicrystalline Block Copolymer Precursors. *Nanoscale* **2013**, *5* (1), 184−192.

(28) Loo, Y.-L.; Register, R. A.; Ryan, A. J. Modes of Crystallization in Block Copolymer Microdomains: Breakout, Templated, and Confined. *Macromolecules* **2002**, *35* (6), 2365−2374.

(29) Voet, V. S. D.; Alberda van Ekenstein, G. O. R.; Meereboer, N. L.; Hofman, A. H.; ten Brinke, G.; Loos, K. Double-Crystalline PLLA-b-PVDF-b-PLLA Triblock Copolymers: Preparation and Crystallization. *Polym. Chem.* **2014**, *5* (7), 2219−2230.

(30) Voet, V. S. D.; ten Brinke, G.; Loos, K. Well-Defined Copolymers Based on Poly(Vinylidene Fluoride): From Preparation and Phase Separation to Application. *J. Polym. Sci., Part A: Polym. Chem.* **2014**, *52* (20), 2861−2877.

(31) Liu, C.-L.; Lin, M.-C.; Chen, H.-L.; Müller, A. J. Evolution of Crystal Orientation in One-Dimensionally Confined Space Templated by Lamellae-Forming Block Copolymers. *Macromolecules* **2015**, *48* (13), 4451−4460.

(32) Guerre, M.; Semsarilar, M.; Godiard, F.; Améduri, B.; Ladmiral, V. Polymerization-Induced Self-Assembly of PVAc-b-PVDF Block Copolymers via RAFT Dispersion Polymerization of Vinylidene Fluoride in Dimethyl Carbonate. *Polym. Chem.* **2017**, *8* (9), 1477−1487.

(33) Guerre, M.; Semsarilar, M.; Totée, C.; Silly, G.; Améduri, B.; Ladmiral, V. Self-Assembly of Poly(Vinylidene Fluoride)-Block-Poly(2-(Dimethylamino)Ethylmethacrylate) Block Copolymers Prepared by CuAAC Click Coupling. *Polym. Chem.* **2017**, *8* (34), 5203−5211.

(34) Voet, V. S. D.; Hermida-Merino, D.; ten Brinke, G.; Loos, K. Block Copolymer Route towards Poly(Vinylidene Fluoride)/Poly(Methacrylic Acid)/Nickel Nanocomposites. *RSC Adv.* **2013**, *3* (21), 7938−7946.

(35) Meereboer, N. L.; Terzić, I.; Saidi, S.; Hermida Merino, D.; Loos, K. Nanoconfinement-Induced β-Phase Formation Inside Poly(Vinylidene Fluoride)-Based Block Copolymers. *ACS Macro Lett.* **2018**, *7*, 863−867.

(36) Terzic, I.; Meereboer, N. L.; Acuautla, M.; Portale, G.; Loos, K. Novel Electroactive Materials with Tunable Response Based on Block Copolymer Self-Assembly. *Nat. Commun.* **2018**, in peer review.

(37) Ranjan, R.; Brittain, W. J. Tandem RAFT Polymerization and Click Chemistry: An Efficient Approach to Surface Modification. *Macromol. Rapid Commun.* **2007**, *28* (21), 2084−2089.

(38) Terzic, I.; Meereboer, N. L.; Loos, K. CuAAC Click Chemistry: A Versatile Approach towards PVDF-Based Block Copolymers. *Polym. Chem.* **2018**, *9*, 3714.

(39) Borsboom, M.; Bras, W.; Cerjak, I.; Detollenaere, D.; Glastra van Loon, D.; Goedtkindt, P.; Konijnenburg, M.; Lassing, P.; Levine, Y. K.; Munneke, B.; et al. The Dutch−Belgian Beamline at the ESRF. *J. Synchrotron Radiat.* **1998**, *5* (3), 518−520.

(40) Bras, W.; Dolbnya, I. P.; Detollenaere, D.; van Tol, R.; Malfois, M.; Greaves, G. N.; Ryan, A. J.; Heeley, E. Recent Experiments on a Small-Angle/Wide-Angle X-Ray Scattering Beam Line at the ESRF. *J. Appl. Crystallogr.* **2003**, *36* (3), 791−794.

(41) Portale, G.; Cavallo, D.; Alfonso, G. C.; Hermida-Merino, D.; van Drongelen, M.; Balzano, L.; Peters, G. W. M.; Goossens, J. G. P.; Bras, W. Polymer Crystallization Studies under Processing-Relevant Conditions at the SAXS/WAXS DUBBLE Beamline at the ESRF. *J. Appl. Crystallogr.* **2013**, *46* (6), 1681−1689.

(42) Guiot, J.; Ameduri, B.; Boutevin, B. Radical Homopolymerization of Vinylidene Fluoride Initiated by Tert-Butyl Peroxypivalate. Investigation of the Microstructure by 19F and 1H NMR Spectroscopies and Mechanisms. *Macromolecules* **2002**, *35* (23), 8694−8707.

(43) Gai, Y.; Lin, Y.; Song, D.-P.; Yavitt, B. M.; Watkins, J. J. Strong Ligand−Block Copolymer Interactions for Incorporation of Relatively Large Nanoparticles in Ordered Composites. *Macromolecules* **2016**, *49* (9), 3352−3360.

(44) Bondzic, S.; de Wit, J.; Polushkin, E.; Schouten, A. J.; ten Brinke, G.; Ruokolainen, J.; Ikkala, O.; Dolbnya, I.; Bras, W. Self-Assembly of Supramolecules Consisting of Octyl Gallate Hydrogen Bonded to Polyisoprene-Block-Poly(Vinylpyridine) Diblock Copolymers. *Macromolecules* **2004**, *37* (25), 9517−9524.

(45) Leibler, L. Theory of Microphase Separation in Block Copolymers. *Macromolecules* **1980**, *13* (6), 1602−1617.

(46) Moon, H. C.; Bae, D.; Kim, J. K. Self-Assembly of Poly(3-Dodecylthiophene)-Block-Poly(Methyl Methacrylate) Copolymers Driven by Competition between Microphase Separation and Crystallization. *Macromolecules* **2012**, *45* (12), 5201−5207.

(47) Lin, M.-C.; Chen, H.-L.; Lin, W.-F.; Huang, P.-S.; Tsai, J.-C. Crystallization of Isotactic Polypropylene under the Spatial Confinement Templated by Block Copolymer Microdomains. *J. Phys. Chem. B* **2012**, *116* (40), 12357−12371.

(48) Lynd, N. A.; Hillmyer, M. A.; Matsen, M. W. Theory of Polydisperse Block Copolymer Melts: Beyond the Schulz−Zimm Distribution. *Macromolecules* **2008**, *41* (12), 4531−4533.

(49) Klein, R. J.; Runt, J.; Zhang, Q. M. Influence of Crystallization Conditions on the Microstructure and Electromechanical Properties of Poly(Vinylidene Fluoride−trifluoroethylene−chlorofluoroethylene) Terpolymers. *Macromolecules* **2003**, *36* (19), 7220−7226.

(50) Bune, A. V.; Fridkin, V. M.; Ducharme, S.; Blinov, L. M.; Palto, S. P.; Sorokin, A. V.; Yudin, S. G.; Zlatkin, A. Two-Dimensional Ferroelectric Films. *Nature* **1998**, *391* (6670), 874−877.

(51) Lutkenhaus, J. L.; McEnnis, K.; Serghei, A.; Russell, T. P. Confinement Effects on Crystallization and Curie Transitions of Poly(Vinylidene Fluoride-Co-Trifluoroethylene). *Macromolecules* **2010**, *43* (8), 3844−3850.

(52) Guan, F.; Wang, J.; Pan, J.; Wang, Q.; Zhu, L. Effects of Polymorphism and Crystallite Size on Dipole Reorientation in Poly(Vinylidene Fluoride) and Its Random Copolymers. *Macromolecules* **2010**, *43* (16), 6739−6748.

(53) Soulestin, T.; Ladmiral, V.; Lannuzel, T.; Domingues Dos Santos, F.; Ameduri, B. Importance of Microstructure Control for Designing New Electroactive Terpolymers Based on Vinylidene Fluoride and Trifluoroethylene. *Macromolecules* **2015**, *48* (21), 7861−7871.

(54) Soulestin, T.; Marcelino Dos Santos Filho, P.; Ladmiral, V.; Totée, C.; Silly, G.; Lannuzel, T.; Domingues Dos Santos, F.; Ameduri, B. Influence of Trans-1,3,3,3-Tetrafluoropropene on the Structure−Properties Relationship of VDF- and TrFE-Based Terpolymers. *Macromolecules* **2017**, *50* (2), 503−514.

(55) Soulestin, T.; Filho, P. M. D. S.; Ladmiral, V.; Lannuzel, T.; Santos, F. D. D.; Améduri, B. Ferroelectric Fluorinated Copolymers

with Improved Adhesion Properties. *Polym. Chem.* **2017**, *8* (6), 1017−1027.

(56) Kuffel, J.; Kuffel, P. *High Voltage Engineering Fundamentals*; Elsevier: 2000.

(57) Tan, S.; Xiong, J.; Zhao, Y.; Liu, J.; Zhang, Z. Synthesis of Poly(Vinylidene Fluoride-co-Chlorotrifluoroethylene)-g-Poly(Methyl Methacrylate) with Low Dielectric Loss by Photo-Induced Metal-Free ATRP. *J. Mater. Chem. C* **2018**, *6* (15), 4131−4139.

(58) Guan, F.; Wang, J.; Yang, L.; Tseng, J.-K.; Han, K.; Wang, Q.; Zhu, L. Confinement-Induced High-Field Antiferroelectric-like Behavior in a Poly(Vinylidene Fluoride-Co-Trifluoroethylene-Co-Chlorotrifluoroethylene)-Graft-Polystyrene Graft Copolymer. *Macromolecules* **2011**, *44* (7), 2190−2199.

(59) Guan, F.; Yang, L.; Wang, J.; Guan, B.; Han, K.; Wang, Q.; Zhu, L. Confined Ferroelectric Properties in Poly(Vinylidene Fluoride-Co-Chlorotrifluoroethylene)-Graft-Polystyrene Graft Copolymers for Electric Energy Storage Applications. *Adv. Funct. Mater.* **2011**, *21* (16), 3176−3188.